Computed and Measured Turbulence in Axisymmetric Reciprocating Engines

F. Grasso* and F. V. Bracco†
Princeton University, Princeton, New Jersey

The turbulence flowfield of a reciprocating engine strongly influences its combustion and is affected by intake system and chamber geometry. Comparisons are presented of computed and measured turbulence near top dead center (TDC), prior to ignition, in two reciprocating engines. The model is for a two-dimensional axisymmetric flowfield and employs a k-ϵ submodel for turbulent transport. The same model constants were used in all computations. For a pancake-like combustion chamber and in the absence of bulk flows, the computed TDC turbulence intensity was compared with that measured by Lancaster vs engine speed, load, and compression ratio. With swirl, computed turbulence and tangential velocities were compared with those measured by Witze at two engine speeds. In good agreement with the experimental data the model reproduces proportionality of TDC turbulence intensity to engine speed, insensitivity to compression ratio, linear dependence on load in the absence of swirl, and insensitivity to load in the presence of swirl. Then, in a parametric study, the effects were identified of quantities not varied in the experiments. Near TDC, for a cup-in-piston chamber with high squish, with or without swirl, two regions exist. Near the edge of the cup, turbulence is dominated by production due to the squish and its intensity is proportional to engine speed but insensitive to load and compression ratio. Near the axis and the bottom of the cup it tends to behave more like the case of no squish.

Nomenclature

b	= velocity of boundary, cm/s
$C_\mu, C_{\epsilon_1}, C_{\epsilon_2}, C_{\epsilon_3}$	= constants in the turbulence model
c_p, c_v	= specific heats, erg/g·K
CD	= cup depth, cm
CL	= TDC clearance, cm
CR	= compression ratio
D	= effective diffusivity, cm²/s
I	= specific internal energy, erg/g
J^k	= mass flux of species k, g/cm²·s
J_q	= energy flux, erg/g·cm²·s
h	= specific enthalpy, erg/g
k	= kinetic energy of turbulence, cm²/s²
n	= normal unit vector
p	= pressure, dyne/cm²
Pr	= Prandtl number
r,z	= coordinate directions, cm
$\Re$	= universal gas constant, erg/mole·K
R	= half bore, cm
R_c	= cup radius, cm
rpm	= engine speed, rev/min
Sc	= Schmidt number
SR	= swirl ratio = angular velocity of swirl divided by angular velocity of the engine
SQ	= squish ratio = $1 - R_c^2/R^2$ = area of piston shoulder divided by area of piston
t	= time, s
t	= tangent unit vector
u	= component of velocity in r direction, cm/s
u	= velocity vector
$\underline{U}$	= unit tensor
v	= component of velocity in z direction, cm/s
$\forall$	= control volume, cm³
$\partial\forall$	= boundary of $\forall$, cm²
w	= component of velocity in tangential direction, cm/s
W	= molecular weight, g/mole
α,β	= constants that determine initial values of k and ϵ
$\Delta r, \Delta z$	= mesh spacing in r and z, cm
ϵ	= dissipation rate of turbulence kinetic energy, cm²/s³
η_v	= volumetric efficiency
θ	= crankangle
θ_i	= initial crankangle, deg
λ	= effective heat conduction coefficient, erg/cm·K·s
μ	= effective viscosity, g/cm·s
ν	= kinematic viscosity, cm²/s
ρ	= density, g/cm³
σ	= effective stress tensor, dyne/cm²
$\underline{\sigma}$	= Prandtl number
ϕ	= general dependent variable

Subscripts

i	= ith direction
LAM	= laminar
TDC	= TDC value
TURB	= turbulent

Superscripts

k	= kth species
T	= transpose
$( )'$	= fluctuating component
$( )^*$	= nondimensional quantity

Received March 15, 1982; revision received July 14, 1982.

*Graduate Student, Department of Mechanical and Aerospace Engineering.
†Associate Professor, Department of Mechanical and Aerospace Engineering. Member AIAA.

Introduction

THE turbulent flowfield of a spark-ignition engine strongly influences its combustion characteristics and is affected by the design of the combustion chamber and the intake system. It is important then to understand the mechanism by which these engine variables affect engine turbulence.

This work explores the influence of chamber design, and engine operating conditions on top dead center (TDC) turbulence prior to ignition. It will be shown that many of the

trends that were identified in earlier studies[1-8] are recovered from a single model. Thus the common causes of these trends are elucidated.

The model employed is for a two-dimensional axisymmetric flowfield. Turbulence is described by a two-equation model for its kinetic energy k and its dissipation rate ϵ. The engine parameters explored are speed (rpm), load (η_v), compression ratio (CR), swirl ratio (SR), and squish (SQ).

In the following sections the model is described, comparisons with experimental data are shown, and predictions are summarized of a parametric study.

Model

Governing Equations

The model describes the fluid motion in a two-dimensional axisymmetric engine. The equations consist of a set of partial differential equations for the conservation of species, momentum, and energy. Two additional equations are solved for the turbulence kinetic energy and its dissipation rate. The governing equations are written in integral form for a control volume $\mathcal{V}(t)$ which is allowed to vary in time with a boundary velocity $\boldsymbol{b}$ to account for the piston motion while still solving the equations in the physical space. The equations are

Conservation of species

$$\frac{\partial}{\partial t}\int_{\mathcal{V}(t)} \rho^k \mathrm{d}\mathcal{V} + \int_{\partial\mathcal{V}} \rho(\boldsymbol{u}-\boldsymbol{b})\cdot\boldsymbol{n}\mathrm{d}s = -\int_{\partial\mathcal{V}} (\boldsymbol{J}^k)\cdot\boldsymbol{n}\mathrm{d}s \tag{1}$$

Conservation of momentum

$$\frac{\partial}{\partial t}\int_{\mathcal{V}(t)} \rho\boldsymbol{u}\mathrm{d}\mathcal{V} + \int_{\partial\mathcal{V}} \rho\boldsymbol{u}(\boldsymbol{u}-\boldsymbol{b})\cdot\boldsymbol{n}\mathrm{d}s = \oint_{\partial\mathcal{V}} \underline{\boldsymbol{\sigma}}\cdot\boldsymbol{n}\mathrm{d}s - \int_{\partial\mathcal{V}} p\boldsymbol{n}\mathrm{d}s + \int_{\mathcal{V}(t)} \rho w^2 \frac{\nabla r}{r}\mathrm{d}\mathcal{V} \tag{2}$$

Conservation of energy

$$\frac{\partial}{\partial t}\int_{\mathcal{V}(t)} \rho I\mathrm{d}\mathcal{V} + \int_{\partial\mathcal{V}} \rho I(\boldsymbol{u}-\boldsymbol{b})\cdot\boldsymbol{n}\mathrm{d}s = -\int_{\partial\mathcal{V}} \boldsymbol{J}_q\cdot\boldsymbol{n}\mathrm{d}s - \int_{\mathcal{V}(t)} p\frac{\nabla\cdot r\boldsymbol{u}}{r}\mathrm{d}\mathcal{V} - \int_{\mathcal{V}(t)} \underline{\boldsymbol{\sigma}}:\nabla\boldsymbol{u}\mathrm{d}\mathcal{V} \tag{3}$$

where $\boldsymbol{J}^k$, $\boldsymbol{\sigma}$, and $\boldsymbol{J}_q$ are the mass flux of species k, the stress tensor, and the heat flux, respectively, and are defined as follows:

$$\boldsymbol{J}^k = -\rho D\nabla\left(\frac{\rho^k}{\rho}\right) \quad \text{(Fick's law)} \tag{4}$$

$$-\underline{\boldsymbol{\sigma}} = \mu(\nabla\boldsymbol{u} + \nabla\boldsymbol{u}^T) - \tfrac{2}{3}\left[\rho k + \mu\frac{\nabla\cdot(r\boldsymbol{u})}{r}\right]\underline{\boldsymbol{U}} \quad \text{(Newton's law)} \tag{5}$$

$$\boldsymbol{J}_q = -\lambda\nabla T - \sum_k h^k\rho D\nabla\left(\frac{\rho^k}{\rho}\right) \quad \text{(Fourier's law)} \tag{6}$$

where $\underline{\boldsymbol{U}}$ is the unit tensor, and μ, ρD, and λ are defined as

$$\mu = \mu_{\mathrm{LAM}} + \rho C_\mu(k^2/\epsilon) \tag{7}$$

$$\rho D = (\rho D)_{\mathrm{LAM}} + (\rho D)_{\mathrm{TURB}} = \mu \tag{8}$$

$$\lambda = \lambda_{\mathrm{LAM}} + \lambda_{\mathrm{TURB}} = c_p\mu \tag{9}$$

having used unit Sc and Pr numbers. The perfect gas equation of state was employed,

$$\rho = \Re T\sum_k \rho^k \Big/ W^k$$

The k-ϵ model has already been extensively used in two-dimensional engine flow[4,9-11] and combustion[12-14] studies. Introduced by Kolmogorov,[15] it was developed further by Spalding and his co-workers.[16,17] It leads to an effective turbulent viscosity

$$\mu_{\mathrm{TURB}} = \rho C_\mu k^2/\epsilon \tag{10}$$

where C_μ is a model constant[16] equal to 0.09. The equation for k is obtained by multiplying the momentum equation by the fluctuating velocity component and taking the long-time average,

$$\frac{\partial}{\partial t}(\rho k) + \frac{1}{r}\nabla\cdot(\rho u k r) = -\rho\overline{u_i' u_k'}\frac{\partial u_i}{\partial x_k} - \nu\overline{\frac{\partial u_i'}{\partial x_k}\frac{\partial u_i'}{\partial x_k}} + \frac{\partial}{\partial x_k}\left(\nu\frac{\partial k}{\partial x_k} - \overline{u_k' k}\right) + \text{higher order terms} \tag{11}$$

By neglecting higher order terms, the integral form of the equation which describes the evolution of k becomes

$$\frac{\partial}{\partial t}\int_{\mathcal{V}(t)} \rho k\mathrm{d}\mathcal{V} + \int_{\partial\mathcal{V}} \rho k(\boldsymbol{u}-\boldsymbol{b})\cdot\boldsymbol{n}\mathrm{d}s = -\int_{\partial\mathcal{V}} \boldsymbol{D}_k\cdot\boldsymbol{n}\mathrm{d}s + \int_{\mathcal{V}(t)} (P^k - D^k)\mathrm{d}\mathcal{V} \tag{12}$$

where P^k is the production of turbulence kinetic energy due to deformation by the mean motion, D^k the dissipation of turbulence kinetic energy due to molecular effects, and $\boldsymbol{D}_k$ the diffusion of turbulence kinetic energy due to both laminar and turbulent transport (see Table 1).

Similarly, the equation for the rate of dissipation of turbulence kinetic energy is obtained by differentiating the momentum equation in space, multiplying the result by $\nu(\partial u_i'/\partial x_\ell)$, and taking the long-time average, thus obtaining the equation,

$$\frac{\partial}{\partial t}\int_{\mathcal{V}(t)} \rho\epsilon\mathrm{d}\mathcal{V} + \int_{\partial\mathcal{V}} \rho\epsilon(\boldsymbol{u}-\boldsymbol{b})\cdot\boldsymbol{n}\mathrm{d}s = -\int_{\partial\mathcal{V}} \boldsymbol{D}_\epsilon\cdot\boldsymbol{n}\mathrm{d}s + \int_{\mathcal{V}(t)} (P^\epsilon - D^\epsilon)\mathrm{d}\mathcal{V} \tag{13}$$

where P^ϵ, D^ϵ, and $\boldsymbol{D}_\epsilon$ are the production, dissipation, and diffusion of ϵ, respectively (see Table 1). The values of all of the model constants are given in Table 2. The ϵ equation differs slightly from the one used by Gosman and Johns,[4] Gosman et al.,[11] and Syed and Bracco[12] who had $C_{\epsilon_3} = +1$, and also from that used by Ramos[7] who had $C_{\epsilon_3} = 0$. The details of our derivation are available in Ref. 18.

Boundary and Initial Conditions

The boundary conditions are

$$(\boldsymbol{u}-\boldsymbol{b})\cdot\boldsymbol{n} = 0 \tag{14}$$

$$(\boldsymbol{u}-\boldsymbol{b})\cdot\boldsymbol{t} = 0 \tag{15}$$

$$\rho D\nabla\left(\frac{\rho^k}{\rho}\right)\cdot\boldsymbol{n} = 0 \tag{16}$$

$$\lambda\nabla T\cdot\boldsymbol{n} \neq 0 \tag{17}$$

$$\frac{\mu}{\sigma_{\phi_\ell}}\nabla\phi_\ell\cdot\boldsymbol{n} = 0 \qquad \begin{matrix}\ell=1,\ \phi_1 = k\\ \ell=2,\ \phi_2 = \epsilon\end{matrix} \tag{18}$$

Table 1 Source terms for Eqs. (12) and (13)

Equation	Dependent variable	P^ϕ	D^ϕ	D_ϕ
Turbulence energy	k	G	$\rho\epsilon$	$-\frac{\mu}{\sigma_k}\nabla k$
Dissipation rate	ϵ	$C_{\epsilon_1}G\frac{\epsilon}{k}$	$C_{\epsilon_2}\frac{\epsilon^2}{k}$	
			$+C_{\epsilon_3}\rho\epsilon\frac{\nabla\cdot(ru)}{r}$	$-\frac{\mu}{\sigma_\epsilon}\nabla\epsilon$

where:

$$G=\mu\left[2\left(\frac{\partial u}{\partial r}\right)^2+2\left(\frac{\partial v}{\partial z}\right)^2+\left(\frac{\partial u}{\partial z}+\frac{\partial v}{\partial r}\right)^2+\left(r\frac{\partial w/r}{\partial r}+\frac{\partial w}{\partial z}\right)^2\right]$$
$$-\frac{2}{3}\frac{\nabla\cdot ru}{r}\left(\rho k+\mu\frac{\nabla\cdot(ru)}{r}\right)$$

Table 2 Constants of k-ϵ model

C_μ	0.09	C_{ϵ_3}	−1.0
C_{ϵ_1}	1.44	σ_k	1.0
C_{ϵ_2}	1.92	σ_ϵ	1.3

Table 3 Engine specifications

	Lancaster's engine	Witze's engine	Cup-in-piston chamber
SQ	0	0	84
CR	6.78, 8.72, 10.55	5.4	12, 16, 21
SR	0	≠0	0, 10
η_v, %	25, 50, 75	100	25, 50, 100
rpm	1000, 1500, 2000	460, 1200	1700, 2400, 4000
Bore, cm	8.26	7.6	12
Stroke, cm	11.43	8.3	12

Equations (14-18) specify no flow through the walls of mass, turbulence kinetic energy and its dissipation rate. The heat flux [Eq. (17)] is evaluated using the "log law of the wall."[4,10,13,16]

The initial conditions were specified as follows. Zero mean velocity or solid-body rotation were used and the thermodynamic variables ρ, p, and T were set equal to their isentropic values at the crankangle at which the computation was started. The turbulence kinetic energy and its dissipation rate were initialized according to

$$k=\alpha_1 U_{\text{IN}}^2 \tag{19}$$

$$\epsilon=\beta_1 U_{\text{IN}}^3 \tag{20}$$

where U_{IN}^2 represents the initial kinetic energy and α_1 and β_1 are constants.

It was further assumed that $U_{\text{IN}}^2 \sim \eta_v^2 \text{rpm}^2$, so that

$$k=\alpha\eta_v^2\text{rpm}^2 \tag{21}$$

$$\epsilon=\beta\eta_v^3\text{rpm}^3 \tag{22}$$

The values for the constants α and β were initially obtained from the measurements of Witze.[3]

The system of governing equations was solved numerically by a modified version of the computer code CONCHAS developed at Los Alamos.[19] CONCHAS was extended to solve the two equations for k and ϵ and modified to solve the angular momentum equation as a scalar equation, i.e., the angular velocity was defined at the center of each computational cell and not at the node points as in the original CONCHAS. The latter modification was found necessary to model the decay of swirling flows properly. The mesh used had 18 cells in the radial direction and 8-20 cells in the axial one. Insensitivity to numerical parameters was checked by repeating some computations with higher resolution and finding negligible effects on the computed quantities.

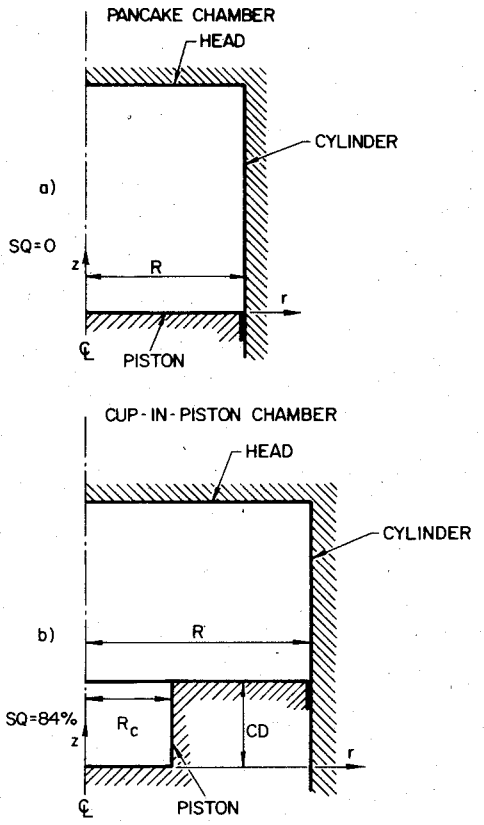

Fig. 1 Engine geometries: a) pancake chamber, b) cup-in-piston chamber.

Results

Comparisons with Measurements

First the computed results were compared with the measurements of Lancaster[2] and with those of Witze, in Johnston et al.,[6] to assess the accuracy of the model.

The engine employed by Lancaster was a single-cylinder, CFR engine, with a pancake-type combustion chamber, i.e., without squish (see Fig. 1) and with negligible swirl. The specifications of the engine are given in Table 3. The experimental data were taken using hot-wire anemometry. Turbulence intensity was measured with a triaxial probe. All measurements were taken at the location where the spark would be in the firing engine. On the assumption that turbulence at TDC is homogeneous, Lancaster justified the use of single-point measurements to characterize the turbulence prior to combustion. The turbulence intensity was defined using a nonstationary analysis. For each engine cycle i, the mean velocity $\bar{U}(t,i)$ was assumed to vary in time and to be equal to the sum of an ensemble-averaged mean velocity $\bar{U}(t)$ and a time-averaged mean velocity for record i, $\bar{U}(i)$, obtained after subtracting $\bar{U}(t)$ from the instantaneous velocity of the i cycle $U(t,i)$. The turbulence intensity was then defined as the rms deviation of $U(t,i)$ from $\bar{U}(t,i)$. The experiments were conducted at three engine speeds, three engine loads, and three compression ratios for a total of seven conditions. The experimental error in the reported velocity fluctuations was estimated by Lancaster to be <20%.

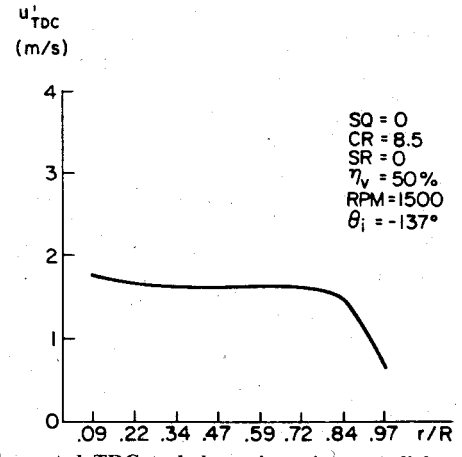

Fig. 2 Computed TDC turbulence intensity vs radial position at $z/CL = 0.4$.

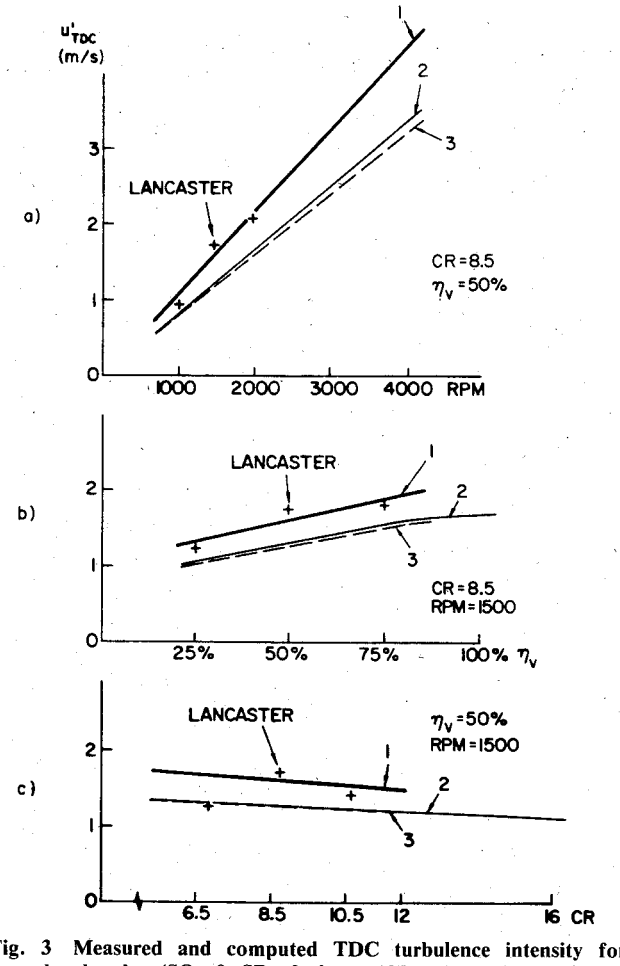

Fig. 3 Measured and computed TDC turbulence intensity for pancake chamber (SQ = 0, SR = 0, $\theta_i = -137$ deg) vs: a) rpm, b) η_v, c) CR.

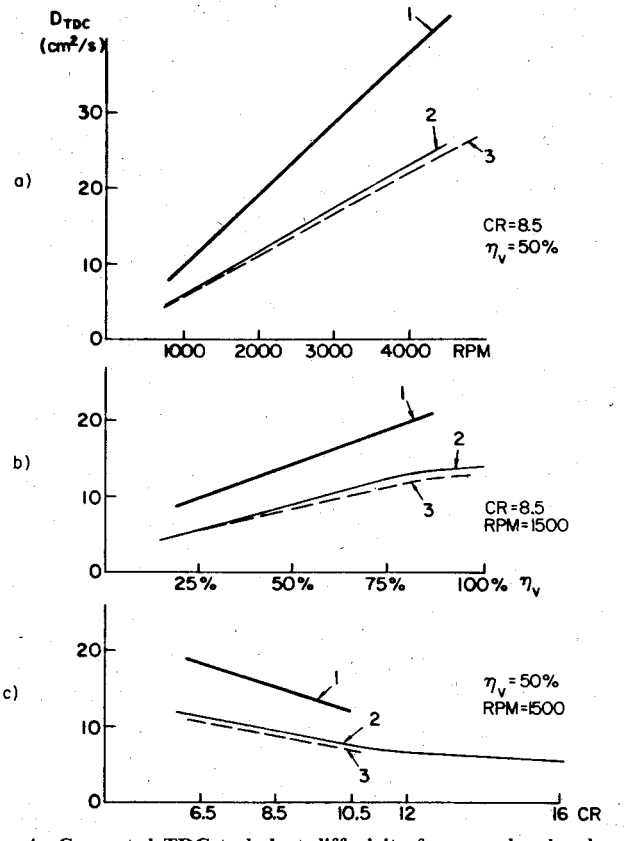

Fig. 4 Computed TDC turbulent diffusivity for pancake chamber (SQ = 0, SR = 0, $\theta_i = -137$ deg) vs: a) rpm, b) η_v, c) CR.

Table 4 Conditions for k and ϵ for comparisons with Lancaster's data[2] ($k = \alpha \text{rpm}^2 \eta_v^2$; $\epsilon = \beta \text{rpm}^3 \eta_v^3$; $D = 0.09k^2/\epsilon$)

Computation	α	β	α^2/β
1	0.61	0.305	1.22
2	0.90	1.22	0.66
3	0.45	0.305	0.66

In all cases the computations were started at -137 deg, i.e., 137 deg before TDC. At TDC the turbulence intensity was defined by the isotropic relation $u' = (\frac{2}{3}k)^{1/2}$, and away from the walls was found to be spatially uniform as shown in Fig. 2. Thus the computed turbulence intensity was averaged across the radius for the comparisons.

In Fig. 3, comparisons between measured and computed TDC turbulence intensities are shown vs rpm, η_v, and CR. For each parameter, three curves (1-3) are given which correspond to different initial values of k and ϵ (see Table 4). In all the computations k and ϵ (and D) were assumed to be initially uniform in space. In computation 3 α and β in Eqs. (21) and (22) were set equal to 0.45 and 0.305, respectively, as deduced from the measurements of Witze[3] so that the ratio α^2/β which defines the initial diffusivity was equal to 0.66. Curve 2 corresponds to the same value of α^2/β but different α and β, whereas curve 1 is for $\alpha^2/\beta = 1.22$. It is seen that the TDC results are sensitive to the initial diffusivity but not to the initial turbulence kinetic energy and its decay rate, i.e., to the initial turbulence lengths and time scales. The best agreement with the data of Lancaster is obtained with $\alpha^2/\beta = 1.22$, whereas from Witze's experiment we deduced $\alpha^2/\beta = 0.66$. Limitations in the quantity and accuracy of available experimental data allows us to conclude only that this ratio appears to be of order 1.0. More importantly, from Fig. 3 we also observe that both the experiments and the computations indicate that TDC turbulence intensity scales linearly with rpm, varies linearly with η_v, and is rather insensitive to compression ratio. Hence k is found to vary as $\eta_v^2 \text{rpm}^2$ at TDC. It may be pointed out that using the k-ϵ model the scaling of turbulence with rpm can be proved analytically.[18] In Fig. 4, the computed diffusivity at TDC is plotted vs rpm, η_v, and CR for $\alpha^2/\beta = 0.66$ and 1.22 (no comparisons are shown since the diffusivity was not measured in the experiment of Lancaster). The model predicts linear variation of the diffusivity vs rpm at all speeds and its increase with η_v and 1/CR. These results are also consistent with a mixing length model for D according to which $D \sim \ell u'$, where

Table 5 Initial conditions for k and ϵ for comparisons with Witze's data[6]

Computation	Expressions	at 460 rpm and $\theta = -160$ deg	Values at 1200 rpm and $\theta = -50$ deg for comp. a and $\theta = -160$ deg for comp. b, c
a	$k = 3/2u'^2$, cm^2/s^2	u' from Witze's data ($=4.2310^4$ at $r/R=0.5$)	u' from Witze's data ($=1.8410^5$ at $r/R=0.5$)
	D, cm^2/s	17.6 (from Robinson's computation)	17.6(1200/460) = 45.9
	$\epsilon = 0.09k^2/D$, cm^2/s^3	From above k and D ($=1.0210^8$ at $r/R=0.5$)	From above k and D ($=7.3610^8$ at $r/R=0.5$)
b	$k = \alpha\,\text{rpm}^2\eta_p^2$	1.2910^5	8.7610^5
	$\epsilon = \beta\,\text{rpm}^3\eta_v^3$	2.3710^7	5.2710^8
	$D = 0.09k^2/\epsilon$	50.2	131
c	$k = \alpha\,\text{rpm}^2\eta_p^2/58.5$	2.210^3	1.510^4
	$\epsilon = \beta\,\text{rpm}^3\eta_v^3/3.4210^3$	8.7310^3	1.5510^5
	$D = 0.09k^2/\epsilon$	50.1	131

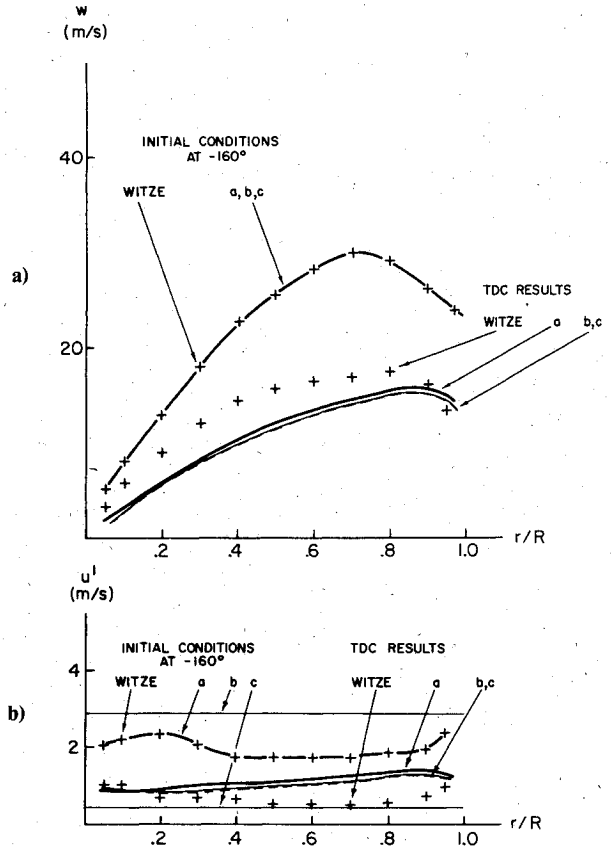

Fig. 5 Measured and computed initial and TDC values of: a) mean tangential velocity, b) turbulence intensity (pancake chamber and 460 rpm).

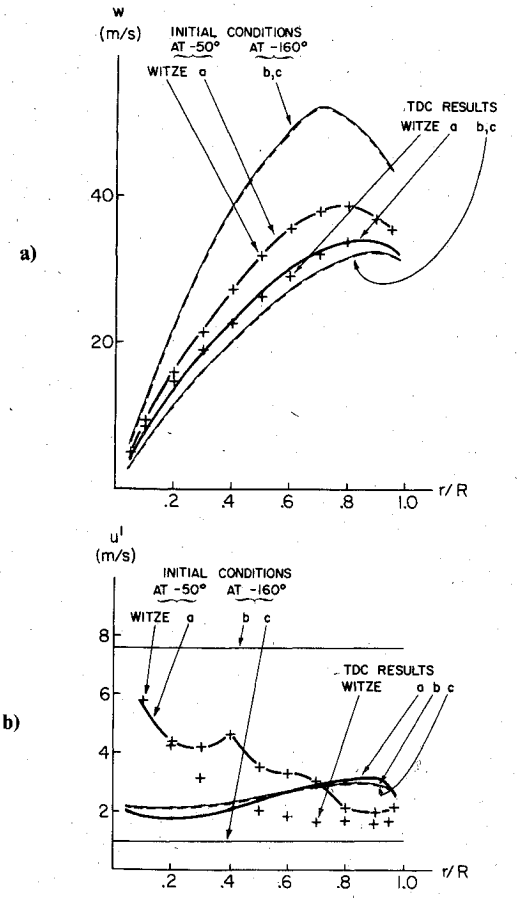

Fig. 6 Measured and computed initial and TDC values of: a) mean tangential velocity, b) turbulence intensity (pancake chamber and 1200 rpm).

ℓ is a mixing length scale and u' the turbulence intensity. If it is assumed that at TDC ℓ is determined by the clearance height, then $D_{\text{TDC}} \sim u'_{\text{TDC}}/(\text{CR}-1) \sim f(\eta_v\text{rpm})/(\text{CR}-1)$, where f is a linear function of $(\eta_v\text{rpm})$, as shown in Fig. 3. Hence ϵ is found to vary as $\eta_v^3\text{rpm}^3(\text{CR}-1)$.

As pointed out earlier, in Lancaster's engine no significant bulk flow was present. Thus a comparison with his data does not assure that the model properly reproduces the decay of organized flows. For that the next comparison is made with the data of Witze[6] that were taken in the presence of strong swirl. The engine employed by Witze was a single-cylinder Teledyne-Wisconsin type of AENL engine, modified by replacing the original cylinder head and valves to provide a simple pancake combustion-chamber shape, as shown in Fig. 1. However, the valves were located in the cylinder wall, thus creating unusual geometrical configuration and valve timing. The specifications of the engine are given in Table 3.

The experimental data were taken using an LDV technique with a dual-beam backscatter optical arrangement. Mean velocity and turbulence intensity were measured at several radial and axial positions. The mean velocity $\bar{U}$ at a given crankangle θ was defined as the ensemble average of all instantaneous values u at crankangles between $\theta - \Delta\theta$ and $\theta + \Delta\theta$. The measurement window $\Delta\theta$ was 2 deg. The tur-

bulence intensity u' was then defined as the rms deviation of the velocity from its mean.[6] The experiments were conducted with a motored engine at two engine speeds.

In Figs. 5 and 6 the computed and measured velocity fluctuations and mean tangential velocity are shown at the two engine speeds of Witze's experiment. At each speed, three computations were performed from different initial conditions (see Table 5).

The data of Witze at the earliest crankangle of the measurements (-160 deg at 460 rpm and -50 deg at 1200 rpm) are not sufficient to specify completely the initial conditions for the computations. When there is no bulk flow, only the values of α and β are needed (and only the ratio α^2/β is important). But with strong bulk flows, it is necessary to know the initial spatial distributions of the mean velocity, turbulence, and rate of decay of the turbulence, i.e., the initial values of w, k, and ϵ. Witze's data provide the initial values of w and k but not of ϵ. The three computations differ in the assumptions made to determine the initial values of ϵ and in other initial conditions.

In computation a, w and k were initialized using the mean velocity and velocity fluctuations measured by Witze at -160 deg for 460 rpm and -50 deg for 1200 rpm ($k=3/2u'^2$) and ϵ using the constant diffusivity of Robinson[6] according to the relationship $\epsilon=0.09k^2/D$. Robinson found that he could reproduce the measured decay of the mean tangential velocity with a uniform and constant diffusivity of $D=17.6$ cm^2/s at 460 rpm (and we set $D=17.6\times1200/460$ at 1200 rpm). The computed TDC mean tangential velocities are in reasonably good agreement with the measured ones at both speeds, but the computed velocity fluctuations differ noticeably, particularly at 1200 rpm.

Noting that the measured mean velocity exhibits a solid-body profile in a significant fraction of the chamber and that the turbulence predicted in computation a tends to be rather uniform within the chamber, in computation b we went back to the spatially uniform initial values of k and ϵ (and, consequently, of D) of Eqs. (21) and (22) that in the absence of swirl had given satisfactory results in the comparisons with Lancaster's data. (From Fig. 5 it can be seen that the initial velocity fluctuation thus predicted at -160 deg for 460 rpm is larger than that measured.) At both engine speeds the computations were then started at -160 deg from Witze's mean velocity at 460 rpm and from a scaled up mean velocity at 1200 rpm since the mean velocity was not measured by Witze at -160 deg for 1200 rpm. The scaling consisted of multiplying the measured mean velocity at 460 rpm by the ratio of measured TDC angular momenta at the two engine speeds, which turns out to be about 1.75 (when a ratio of 2.00 is used, the results change somewhat but not the general trends and conclusions). In Figs. 5 and 6 it can be seen that both the mean and the fluctuating TDC velocities predicted with this set of initial conditions are very similar to those predicted with the previous one.

Finally, in computation c we kept the same value of the initial diffusivity as in computation b but reduced the initial values of k and ϵ to bring the values of the velocity fluctuations closer to those measured by Witze at -160 deg for 460 rpm. From the figures, it can be seen that the predicted TDC velocity and velocity fluctuations are again very similar to those of computations a and b.

In conclusion, even though the Lancaster and Witze engines are very different in their configurations and operating conditions, acceptable results were obtained for both engines with the same model and model constants. Particularly interesting is the relative influence of the initial values of k, ϵ, and D on the TDC flowfield.

In Lancaster's engine strong bulk flows were absent and TDC turbulence intensity and diffusivity were found to be insensitive to the initial values of k and ϵ. But when the initial value of D was increased by a factor of two, the TDC values increased by a factor of about 1.5.

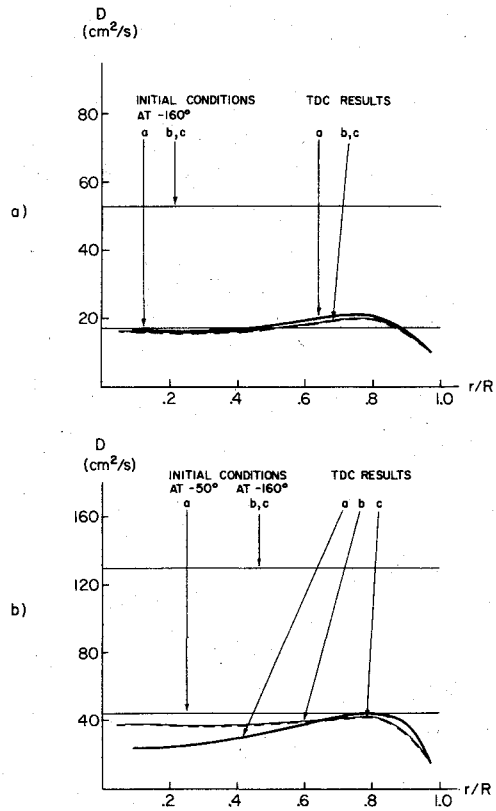

Fig. 7 Computed initial and TDC values of the diffusivity: a) 460 rpm, b) 1200 rpm.

In Witze's engine the strong swirl had a dominating effect. During compression it decayed but also generated additional turbulence and at TDC the diffusivity was 2-4 times larger than in Lancaster's engine. Thus the details of the initial turbulence were even less important. The TDC flowfield was completely insensitive to the initial values of k and ϵ and not strongly effected even by the initial value of D (see Fig. 7). Thus computations b and c gave essentially the same TDC results, starting from the same diffusivities and from turbulent kinetic energies differing by a factor of 60 and rates of decay differing by 3600. And computations a and b gave again similar TDC results starting from initial diffusivities that differ by a factor of three.

Effect of Swirl and Squish

The comparisons with Lancaster's and Witze's data served to evaluate the accuracy of the model and to isolate certain trends. But these comparisons involved only a simple chamber without squish and, even then, in Lancaster's data the load and compression ratio were changed in the absence of swirl, whereas in Witze's data only the engine speed was varied in the presence of swirl. For practical applications it is important to know also the possible effects on the swirl of changes in load and compression ratio, the effects of squish, and the combined effects of squish, swirl, speed, load, and compression ratio. Thus a parametric study was undertaken in which 21 configurations were studied that varied in squish, swirl, speed, load, and compression ratio (see Table 6). All computations were started at -137 deg and k and ϵ were initialized according to Eqs. (21) and (22) (with $\alpha=0.61$ and $\beta=0.305$). When swirl was present, an initial solid-body profile was used. In studying the results, particular attention was paid to the TDC variations of the turbulence intensity, the tangential velocity, and the diffusivity, since the first two are measurable quantities and the last influences the combustion rate the most. The main results are illustrated in some 60 figures that are available in Ref. 18. Because of space limitations, only the main trends are summarized here.

Table 6 Conditions of the parametric study

SQ	CR	SR	η_v, %	rpm
0	8.5	10	50	1500
				2000
				4000
			25	1500
			75	
	6.5		50	
	10.5		50	
84	21	0	100	1700
				2400
				4000
			25	1700
			50	
	12		100	
	16		100	
84	21	10	100	1700
				2400
				4000
			25	1700
			50	
	12		100	
	26		100	

For a pancake chamber and initial solid-body swirl, a boundary layer develops at the walls during compression, the solid-body profile is modified, and turbulence is produced by the tangential shear stresses.

For sufficiently strong swirl, the turbulence thus generated overcomes intake turbulence by the time TDC is reached. Notice that for the same rotational kinetic energy, if the initial swirl profile is not solid body, more turbulence is generated during compression everywhere in the field. This in turn will increase the decay of the tangential velocity during compression but will increase the combustion rate. Since faster combustion is the main reason for inducing swirl in engines, it follows that much more emphasis should be put on the profile of the swirl than on the swirl number. The computations also show that the TDC turbulence intensity and tangential velocity still scale with engine speed and are rather independent of load and compression ratio. The TDC diffusivity is found to vary in accord with $D_{TDC} \sim \ell u'_{TDC}$ in that it changes linearly with engine speed, is rather insensitive to load, and decreases with increasing compression ratio.

With high squish, as for the cup-in-piston configuration of Fig. 1b, and without swirl turbulence is generated near TDC in the shear regions of the squish flow. Since the squish-induced velocity is proportional to the engine speed, TDC turbulence intensity and diffusivity still scale with rpm. In regions where the squish is strongly felt, as in the upper part of the cup near the lip, the effect of load and compression ratio on TDC turbulence intensity and diffusivity is minimal. Where the squish is felt least, as at the bottom of the cup, TDC turbulence intensity and diffusivity tend to follow the trends exhibited by the decaying intake turbulence of pancake-type chambers. In particular the diffusivity decreases with increasing compression ratio. Although the above trends have been observed experimentally,[5] the influence of squish turbulence in various regions of the cup is likely to be a function not only of the squish number (which in our study was at the high end of the practical range), but also of the geometry of the cup (which in our study was not varied).

When engine speed, load, and compression ratio were changed in the presence of both strong swirl and strong squish, it was found that turbulent intensity, tangential velocity, and diffusivity again scale proportionally to engine speed. The same quantities were found to be insensitive to load and to compression ratio except for the diffusivity, which again decreased with increasing compression ratio in the center and bottom of the cup where the effects of squish and swirl are felt least in the simple-cup geometry considered.

Acknowledgments

Support for this work was provided by the U.S. Department of Energy (Contract DE-AC-04-81AL16338), the National Science Foundation (Grant NAG3-8), General Motors, Volkswagenwerk, FIAT, and Komatsu. These results were presented at the 12th DISC Meeting, General Motors Research Laboratories, Warren, Mich., October 1980 and orally at the 1981 SAE Automotive Engineering Congress, Detroit, Mich., February 1981.

References

[1] Semenov, E. S., "Studies of Turbulent Flows in Piston Engines," NASA TTF-97, 1963.

[2] Lancaster, D. R., "Effects of Engine Variables on Turbulence in a Spark-Ignition Engine," SAE Paper 760159, Feb. 1976.

[3] Witze, P. O., "Measurements of the Spatial Distribution and Engine Speed Dependence of Turbulent Air Motion in an I. C. Engine," SAE Paper 770220, Feb. 1977.

[4] Gosman, A. D. and Johns, R. J. R., "Development of a Predictive Tool for In-Cylinder Gas Motion in Engines," SAE Paper 780315, Feb. 1978.

[5] Brandl, F., Reverencic, J., Cartellieri, W., and Dent, J. C., "Turbulent Air Flow in the Combustion Bowl of a D. I. Diesel Engine and Its Effect on Engine Performance," SAE Paper 790040, Feb. 1979.

[6] Johnston, S. C., Robinson, C. W., Rorke, W. S., Smith, J. R., and Witze, P. O., "Application of Laser Diagnostics to an Injected Engine," SAE Paper 790092, Feb. 1979 (see also Sandia National Laboratories, Rept. SAND81-8242, 1981.

[7] Ramos, J. I., "Axisymmetric Flow Fields in Motored and Firing Spark-Ignition Engines," Ph.D. Thesis 1473-T, Dept. of Mech. and Aero. Eng., Princeton Univ., Princeton, N. J., March 1980.

[8] Coghe, A. et al., "Velocity Measurements in the Motored Single Cylinder FIAT Engine," Paper presented at Workshop on Combustion in Reciprocating Engines, Rome, Dec. 1980.

[9] Gosman, A. D. and Watkins, A. P., "A Computer Prediction Method for Turbulent Flow and Heat Transfer in Piston Cylinder Assemblies," Paper presented at Symposium on Turbulent Shear Flow, Pennsylvania State University, University Park, Pa., April 1977.

[10] Ramos, J. I., Humphrey, J. A. C., and Sirignano, W. A., "Numerical Prediction of Axisymmetric, Laminar and Turbulent Flows in Motored, Reciprocating Internal Combustion Engines," *SAE Transactions,* Vol. 88, 1979, pp. 1217-1242.

[11] Gosman, A. D., Johns, R. J. R., and Watkins, A. P., "Development of Prediction Methods for In-Cylinder Processes in Reciprocating Engines," *Combustion Modeling in Reciprocating Engines,* edited by J. N. Mattavi and C. A. Amann, Plenum Press, New York, 1980, pp. 69-124.

[12] Syed, S. A. and Bracco, F. B., "Further Comparisons of Computed and Measured Divided-Chamber Engine Combustion," SAE Paper 790247, Feb. 1979.

[13] Grasso, F. and Bracco, F. V., "Evaluation of a Mixing-Controlled Model for Engine Combustion," oral presentation at SAE Congress, 1980, and *Combustion Science and Technology,* Vol. 28, 1982, pp. 185-210.

[14] Ahmadi-Befrui, B., Gosman, A. D., Lockwood, F. C., and Watkins, A. P., "Multidimensional Calculation of Combustion in an Idealized Homogeneous Charge Engine: A Progress Report," SAE Paper 810051, Feb. 1981.

[15] Kolmogorov, A. N., "A Refinement of Previous Hypothesis Concerning the Local Structure of Turbulence in a Viscous Incompressible Fluid at High Reynolds Number," *Journal of Fluid Mechanics,* Vol. 13, 1962, pp. 82-85.

[16] Launder, B. E. and Spalding, D. B., "The Numerical Computations of Turbulent Flows," *Computer Methods in Applied Mechanics and Engineering,* Vol. 3, 1974, pp. 269-289.

[17] Hanjalic, K. and Launder, B. E., "A Reynolds Stress Model of Turbulence and Its Application to Thin Shear Flows," *Journal of Fluid Mechanics,* Vol. 52, 1972, Pt. 4, pp. 609-638.

[18] Grasso, F., "On Flows in Internal Combustion Engines," Ph.D. Thesis 1537-T, Dept. of Mech. and Aero. Eng., Princeton Univ., Princeton, N. J., Nov. 1981.

[19] Butler, T. D., Cloutman, L. D., Dukowicz, J. K., and Ramshaw, J. D., "CONCHAS: An Arbitrary Lagrangian-Eulerian Computer Code for Multicomponent Chemically Reactive Fluid Flow at All Speeds," Los Alamos Scientific Laboratory, Los Alamos, N. Mex., Informal Rept. LA-8129-MS, Nov. 1979.